RSC Advances

PAPER

View Article Online
View Journal | View Issue

Cite this: *RSC Adv.*, 2023, **13**, 14974

Terbium-doped carbon dots (Tb-CDs) as a novel contrast agent for efficient X-ray attenuation†

Anara Molkenova, ‡[a] Lazzat Serik,‡[b] Alina Ramazanova,[c] Kamila Zhumanova, [b] Bakyt Duisenbayeva,[d] Ainur Zhussupbekova, [e] Kuanysh Zhussupbekov, [e] Igor V. Shvets,[e] Ki Su Kim, [agh] Dong-Wook Han [f] and Timur Sh. Atabaev *[b]

Received 12th February 2023
Accepted 25th April 2023

DOI: 10.1039/d3ra00958k

rsc.li/rsc-advances

Metal-doped carbon dots have attracted considerable attention in nanomedicine over the last decade owing to their high biocompatibility and great potential for bioimaging, photothermal therapy, and photodynamic therapy. In this study, we prepared, and for the first time, examined terbium-doped CDs (Tb-CDs) as a novel contrast agent for computed tomography. A detailed physicochemical analysis revealed that the prepared Tb-CDs have small sizes (~2–3 nm), contain relatively high terbium concentration (~13.3 wt%), and exhibit excellent aqueous colloidal stability. Furthermore, preliminary cell viability and CT measurements suggested that Tb-CDs exhibit negligible cytotoxicity toward L-929 cells and demonstrate high X-ray absorption performance (~48.2 ± 3.9 HU L g^{-1}). Based on these findings, the prepared Tb-CDs could serve as a promising contrast agent for efficient X-ray attenuation.

1. Introduction

A noninvasive medical imaging system, such as computed tomography (CT), has emerged as a powerful technique for observing, estimating, and characterizing pathological processes for accurate disease diagnosis. In general, CT can easily distinguish between hard tissues and soft tissues but small changes in soft tissues, such as tumors and lesion formations, are difficult to detect due to similar X-ray attenuation properties.[1] Hence, the administration of radiocontrast agents with high X-ray attenuation efficiency is required to collect useful information from the region of interest and to achieve a better signal-to-noise ratio. As a matter of fact, elements with a high atomic number (Z) absorb X-rays more effectively.[1] To date, the clinically approved radiocontrast agents, such as iohexol, iopromide, iobitridol, and some others, are all based on iodine element ($Z = 53$, K-edge ~33.2 keV).[2] The X-ray attenuation efficiency of these iodinated contrast agents is highly dependent on their molecular structure and manufacturer. For example, it was shown that iohexol has an X-ray attenuation efficiency of ~6.5 HU mL mg^{-1} at 120 kV,[3] while iobitridol exhibits a value of ~31.8 HU mL mg^{-1} at 120 kV.[4] Despite recent progress in toxicity reduction, iodinated contrast agents are frequently associated with contrast-induced acute kidney injury and a variety of other side effects.[5,6] Hence, the search for nontoxic and efficient radiocontrast agents is of vital significance.

In the last decade, several Au, Bi, Gd, and Yb element-based nanostructures have been proposed and extensively tested because of their efficient X-ray attenuation properties.[7,8] However, the use of hazardous reagents and solvents during the synthesis, as well as the high product cost, size control difficulty, post-synthetic surface-functionalization, and leaching of metal ions are major obstacles limiting their potential clinical applicability. In this regard, the utilization of metal-doped carbon dots (CDs) appears to be an ideal solution. First of all, a desired metal dopant can be incorporated into the core of CDs during the synthesis process, while the abundance of surface functional groups leads to the stabilization of the prepared colloidal solutions. Secondly, metal-doped CDs are typically prepared in aqueous solutions, which is regarded as a "green" approach. Finally, numerous studies have revealed that metal-doped CDs are less toxic as compared to metal-based nanostructures.[9,10] Therefore, CDs doped with heavy elements, such as Ba ($Z = 56$), Gd ($Z = 64$), Dy ($Z = 66$), Yb ($Z = 70$), Hf ($Z = 72$), and Bi ($Z = 83$), have been extensively studied recently as

[a]*Institute of Advanced Organic Materials, Pusan National University, Busan 46241, Republic of Korea*
[b]*Department of Chemistry, Nazarbayev University, Astana 010000, Kazakhstan. E-mail: timur.atabaev@nu.edu.kz*
[c]*Department of Biology, University of Padua, Padua 35121, Italy*
[d]*Department of Radiology, Republican Diagnostic Center, Astana 010000, Kazakhstan*
[e]*School of Physics, Centre for Research on Adaptive Nanostructures and Nanodevices (CRANN), Trinity College Dublin, Dublin, Ireland*
[f]*Department of Cogno-Mechatronics Engineering, Pusan National University, Busan 46241, Republic of Korea*
[g]*School of Chemical Engineering, College of Engineering, Pusan National University, 2 Busandaehak-ro 63beon-gil, Geumjeong-gu, Busan 46241, Republic of Korea*
[h]*Department of Organic Material Science & Engineering, Pusan National University, 2 Busandaehak-ro 63beon-gil, Geumjeong-gu, Busan 46241, Republic of Korea*

† Electronic supplementary information (ESI) available. See DOI: https://doi.org/10.1039/d3ra00958k

‡ These authors contributed equally.

potential new CT contrast agents.[4,11–14] Regardless of the recent advancements in this field, the development of novel radiocontrast agents still remains an actual task. In this study, for the first time, we investigated the potential of terbium-doped CDs (Tb-CDs) as novel CT contrast agent. Preliminary findings revealed that Tb-CDs are biocompatible and have high X-ray attenuation efficiency that is better than some other metal-doped CDs.

2. Materials and methods

Dextrose (≥99.5%) and terbium chloride hexahydrate ($TbCl_3 \cdot 6H_2O$, 99.9%) were purchased from Merck and used as received. In a typical synthesis procedure, a mixture of 0.25 g of glucose, and ~37.3 mg (0.1 mM) of $TbCl_3 \cdot 6H_2O$ was dissolved in 10 mL of deionized (DI) water and transferred into a 25 mL Teflon-lined autoclave reactor. Then, the temperature of the autoclave was raised slowly to 200 °C in an air oven at a ramping speed of 5 °C min^{-1} and kept for 6 hours at 200 °C. After the synthesis completion, the reactor was allowed to cool naturally to room temperature. The resultant solution was purified from aggregates by passing through a syringe filter with a 0.1 μm pore size and dialyzed against DI water for an appropriate time. Finally, the lyophilization technique was employed to obtain the solvent-free sample, which was used for further characterization.

Fourier-transform infrared vibrational spectroscopy analysis was performed with a dried powder on a Nicolet iS5 FTIR (FT-IR, Thermo Fisher Scientific Inc., Waltham, MA, USA). The sign and magnitude of the zeta potential were measured on a Nanotrac Wave II Q (Microtrac MRB, Haan, Nordrhein-Westfalen, Germany) using an aqueous solution of Tb-CDs (100 ppm). The terbium content was determined by inductively coupled plasma optical emission spectroscopy ICP-OES (Thermo Fisher Scientific iCAP 6300 Duo, USA). In brief, a certain concentration of Tb-CDs was diluted in nitric acid to leach out Tb ions, the excess acid was evaporated, and the resulting salt was dissolved in DI water for analysis. Qualitative and quantitative information on the samples was obtained under an ultra-high vacuum (5×10^{-11} mbar) regime using X-ray photoelectron spectroscopy (XPS) analysis, which was conducted on an Omicron MultiProbe XPS instrument with a dried powder of Tb-CDs. High-resolution spectra were recorded at pass energy of 50 eV, which was realized utilizing a monochromatic Al Kα source (XM 1000, 1486.6 eV) with an overall instrumental resolution of 0.6 eV. The sample fluorescence efficiency was estimated through absolute quantum yield (QY) measurements using a C9920-02 spectrophotometer (Hamamatsu Photonics K.K., Hamamatsu, Japan) using an aqueous solution of Tb-CDs (100 ppm). The murine fibroblast L929 cell line was deployed for cytotoxicity assessment. Concentration-dependent X-ray attenuation characteristics of the prepared nanoprobe were investigated using the clinical computed tomography (CT) instrument (Philips Brilliance 64, Amsterdam, Netherlands). Tb-CD aqueous solutions with various amounts of Tb (with respect to their mass in Tb-CDs) were prepared and examined for X-ray attenuation. Phantom images were acquired from conventional CT parameters: X-ray tube voltage = 120 kV and field of view (FOV) = 200.0 mm.

The L929 cell line was purchased from the Korean Cell Line Bank (Seoul, Korea). The viability of L929 cells in the presence of

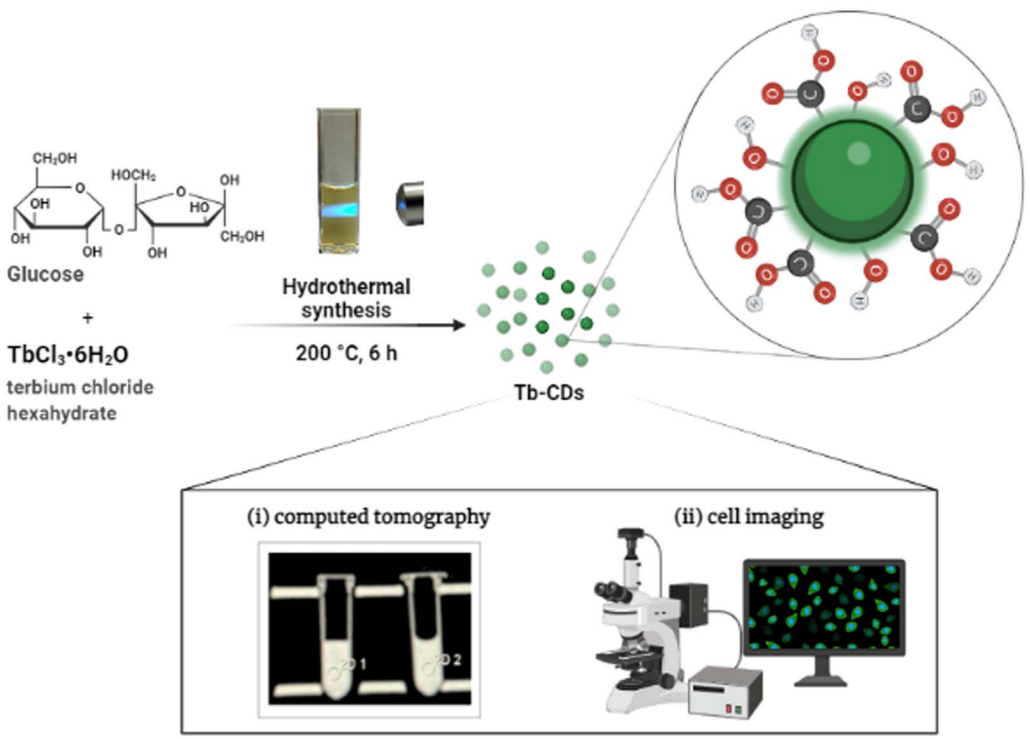

Fig. 1 Synthesis route of Tb-CDs.

Tb-CDs was quantified using the CCK-assay according to the manufacturer's protocol. Optical measurements were performed using an Olympus IX82-F72 fluorescence microscope (Olympus LS, Tokyo, Japan). All measurement conditions and statistical analysis were similar to our previously reported protocol.[15]

3. Results and discussion

To incorporate terbium dopant into the carbon structure, we performed the synthesis of CDs in the presence of terbium ions using a versatile hydrothermal method (Fig. 1). The prepared samples were purified to remove the unreacted reagents. To verify the successful dopant incorporation, the Tb content was quantified using ICP-OES analysis and was found to be 13.3 wt%.

Transmission electron microscopy (TEM) image (inset) and size distribution analysis in Fig. 2A revealed that dextrose-derived Tb-CDs were homogeneous with the average size ranging from 2 nm to 3 nm. As can be seen in Fig. 2B, the Tb-CDs composition was further examined using the recorded FTIR spectrum, demonstrating the presence of various functional groups. The broad peak around 3212 cm^{-1} is ascribed to the O–H stretching vibrations followed by stretching vibration at 2945 cm^{-1}, likely originating from the C–H bond in aliphatic hydrocarbons. The absorption bands at 1725 cm^{-1}, 1582 cm^{-1} and 1040 cm^{-1} could be attributed to the stretching vibrations of C=O, C=C, and C–O–C, respectively. Other absorption peaks were derived from bending vibrations of the C–H bond, such as 1373 cm^{-1}, 1198 cm^{-1}, and 860 cm^{-1}. The FTIR results suggest that the rich content of hydrophilic groups, *e.g.* –COOH and –OH, at the surface of Tb-CDs promoted their solubilization and stabilization in an aqueous medium.[11] This is in good agreement with the zeta potential measurement results (−97.7 mV), suggesting their potential colloidal stability in the physiological environment. The insights into the photophysical properties were further gained from excitation–emission-dependent PL profiles. Fig. 2C demonstrates that the PL emission of Tb-CDs apparently red-shifts when excited by the wavelength varying from 320 to 380 nm. Tb-CDs have an emission maximum at 442 nm with an absolute quantum yield of ~1.4%, which was triggered by the excitation wavelength of 340 nm. CDs typically display excitation-dependent optical properties *via* multiple emission centers such as surface groups, conjugated sp^2 domains in carbon cores, organic fluorophores, and cross-linked polymer chains.[16] Hence, our findings suggest

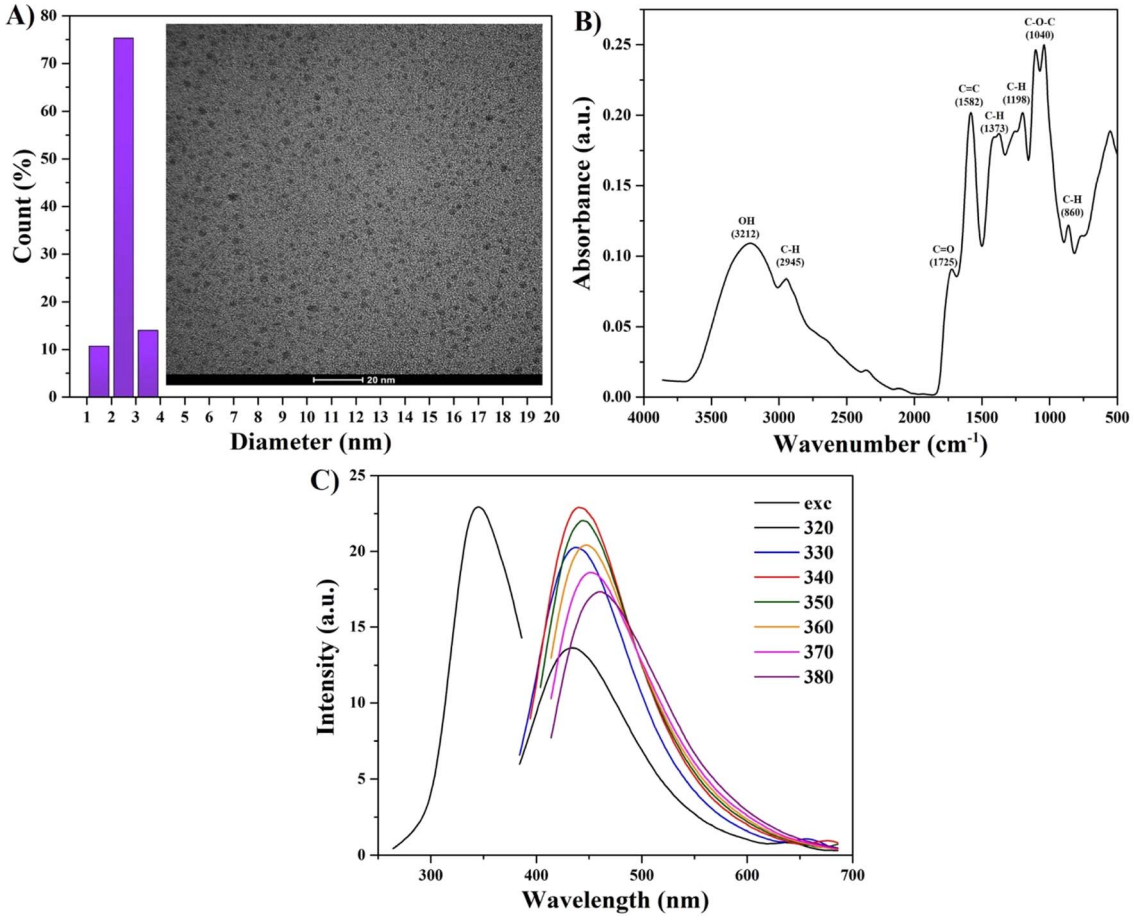

Fig. 2 (A) TEM image and size distribution of Tb-CDs. The scale bar is 20 nm. (B) FTIR spectrum of Tb-CDs. (C) PL excitation and excitation-dependent emission of Tb-CDs.

that the color of Tb-CD emission can be tuned, which could open up new avenues for cell imaging. For example, various fluorescent nanostructures are commonly employed for optical cell labeling.[17–21] Consequently, Tb-CDs can be also employed as a blue or green fluorescent probe for optical labeling (Fig. S1, ESI†).

Next, the structural surface characteristics of the Tb-CDs were explored based on the data retrieved from the XPS analysis. Fig. 3A displays the full-range XPS spectrum exhibiting a weak peak of terbium 4d and distinct peaks of oxygen 1s and carbon 1s. The high-resolution XPS spectra of the C 1s band (Fig. 3B) could be deconvoluted into three main peaks at 288.4 eV, 285.5 eV, and 284.6 eV featuring the presence of C=O, C–O, and C–C/C=C groups, respectively.[4] The high-resolution O 1s spectrum shown in Fig. 3C could be deconvoluted into two characteristic peaks at 532.7 eV and 531.9 eV, which represent C–O and C=O groups, respectively.[22] The high-resolution Tb 4d spectrum shown in Fig. 3D displays a well-resolvable peak centered at 153 eV, which arises from Tb^{4+}.[23] It should be noted that our results are also in good agreement with that of Tb-doped carbon dots produced from folic acid.[24] Furthermore, a small deconvoluted peak at 147.5 eV can be assigned to the Tb^{3+} state.[25] Due to the energetic overlap of Tb 3d and Auger peaks, resolving of the Tb 3d region is not possible, which could be attributed to the limitations of the equipment.

Generally, a high atomic number is a crucial prerequisite for the development of a CT contrast agent with sufficient X-ray attenuation ability. In this regard, terbium ions with inherently high K-edge absorption value of ~52.0 keV (ref. 2) can feasibly serve to produce contrast enhancements that could be observed at typical clinical voltage settings. Currently, CT imaging relies on conventional contrast agents, such as iodine (33.2 keV) and barium based (37.4 keV) compounds, which are restricted by their low K-edge energies for generating satisfying contrast.[26] Consolidating the literature findings above and inspired by the remarkable properties of the terbium element, we performed CT X-ray attenuation measurements of the prepared Tb-CDs. The probe concentration was adjusted based on the Tb content and evaluated over the range of concentrations between 0.3 and 1.2 mg of Tb ions per mL against DI water, which was set as a blank control (HU = 0). Fig. 4 demonstrates the phantom images and the slope of the HU values against the mass of Tb ions. Our findings suggest, that the Tb-CD nanoprobe demonstrated a CT attenuation efficiency of 48.2 ± 3.9 HU mL mg^{-1}, which is higher or comparable to recently published data for commercial iohexol (~6.5 HU mL mg^{-1}), iobitridol (31.83 HU mL mg^{-1}) or Gd and Yb-codoped CDs (45.43 HU mL mg^{-1}) at the same voltage settings.[3,4]

Next, the biocompatibility of Tb-CDs was evaluated using a CCK assay. L929 cells were cultured and co-incubated with

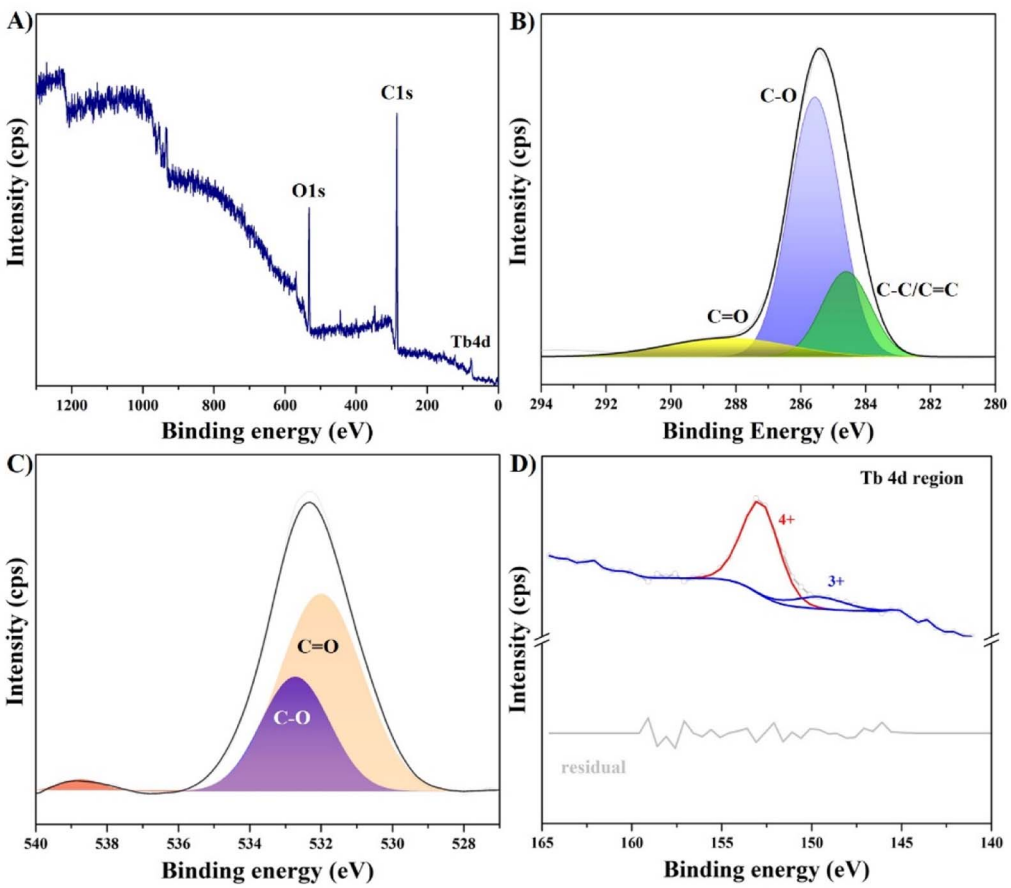

Fig. 3 (A) XPS survey and narrow scan spectra of (B) C 1s, (C) O 1s, and (D) Tb 4d regions of Tb-CDs.

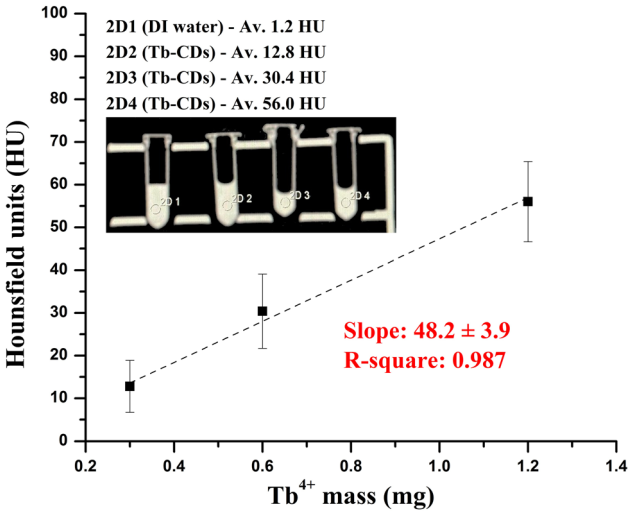

Fig. 4 CT phantom photograph and HU values of Tb-CDs as a function of different Tb ion masses in DI water.

different concentrations (0–200 ppm) of Tb-CDs to assess their cytotoxicity. Fig. 5 shows that the Tb-CDs exhibited a dose-dependent cell viability profile. Notably, Tb-CDs induced no obvious cytotoxicity at the concentration range of 0–200 ppm, suggesting their acceptable biosafety at the cellular level according to the ISO 10993-5 standard.[27] Additionally, the absence of morphology alteration in L929 cells at concentrations as high as 200 ppm further confirmed the biocompatibility of Tb-CDs (Fig. S2, ESI†). In general, the cell membrane is negatively charged, hence, we can speculate that negatively charged Tb-CDs have negligible cellular uptake. However, different cells have different characteristics and functions, hence, they may react differently to the same Tb-CDs.[28] Thus, it should be noted that Tb-CDs can be potentially toxic to other cells/tissues; therefore, further research into Tb-CDs toxicity should be conducted. Furthermore, Tb-CDs should be studied *in vivo* using a small animal model to assess the potential distribution, X-ray attenuation, and clearance pathways of these nanoprobes. It is expected that these questions will be addressed in future studies.

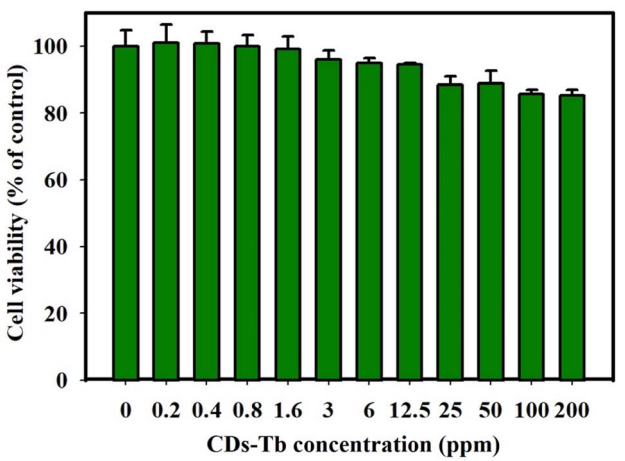

Fig. 5 Cell viability testing of Tb-CDs at varied concentrations of 0–200 ppm.

4. Conclusions

In this study, we investigated the potential applicability of Tb-CDs for effective CT X-ray attenuation. We showed that the prepared Tb-CDs are ultrasmall (~2–3 nm), and have excellent aqueous dispersibility and acceptable biocompatibility. More importantly, the intrinsic X-ray attenuation ability of Tb-CDs was found to be higher than conventional iodine-based contrast agents such as iohexol and iobitridol. In addition to the encouraging results, more extensive research into biosafety of Tb-CDs is required to make further progress in clinical translations.

Conflicts of interest

None declared.

Acknowledgements

This study was financially supported by the 2022 Post-Doc. Development Program of Pusan National University. This work was implemented within the National Research Foundation of Korea (NRF) grant supported by the Korean government (the Ministry of Science and ICT) (No. 2022R1C1C1009533 and 2021M3H4A4079509) and a grant (HF21C0156) of the Korea Health Technology R&D Project through the Korea Health Industry Development Institute (KHIDI), funded by the Ministry of Health and Welfare, Republic of Korea. A. Z. and K. Z. would like to acknowledge funding from IRC through GOIPD/2022/443 and GOIPD/2022/774 awards.

References

1 H. Lusic and M. W. Grinstaff, X-ray computed tomography contrast agents, *Chem. Rev.*, 2013, **113**, 1641–1666.
2 **https://skuld.bmsc.washington.edu/scatter/AS_periodic.html**.
3 V. Harsaker, K. Jensen, H. K. Andersen and A. C. Martinsen, Quantitative benchmarking of iodine imaging for two CT spectral imaging technologies: A phantom study, *European Radiology Experimental*, 2021, **5**, 24.
4 Y. Zhao, X. Hao, W. Lu, R. Wang, X. Shan, Q. Chen, G. Sun and J. Liu, Facile preparation of double rare earth-doped carbon dots for MRI/CT/FI multimodal imaging, *ACS Appl. Nano Mater.*, 2018, **1**, 2544–2551.
5 E. Seeliger, M. Sendeski, C. S. Rihal and P. B. Persson, Contrast-induced kidney injury: mechanisms, risk factors, and prevention, *Eur. Heart J.*, 2012, **33**, 2007–2015.
6 A. L. Faucon, G. Bobrie and O. Clement, Nephrotoxicity of iodinated contrast media: From pathophysiology to prevention strategies, *Eur. J. Radiol.*, 2019, **116**, 231–241.

7 N. Aslan, B. Ceylan, M. M. Koc and F. Findik, Metallic nanoparticles as X-ray computed tomography (CT) contrast agents: A review, *J. Mol. Struct.*, 2020, **1219**, 128599.
8 J. C. Hsu, L. M. Nieves, O. Betzer, T. Sadan, P. B. Noel, R. Popovtzer and D. P. Cormode, Nanoparticle contrast agents for X-ray imaging applications, *WIREs Nanomedicine and Nanobiotechnology*, 2020, **12**, e1642.
9 M. Havrdova, K. Hola, J. Skopalik, K. Tomankova, M. Petr, K. Cepe, K. Polakova, J. Tucek, A. B. Bourlinos and R. Zboril, Toxicity of carbon dots – effect of surface functionalization on the cell viability, reactive oxygen species generation and cell cycle, *Carbon*, 2016, **99**, 238–248.
10 A. Truskewycz, H. Yin, N. Halberg, D. T. H. Lai, A. S. Ball, V. K. Truong, A. M. Rybicka and I. Cole, Carbon dot therapeutic platforms: Administration, distribution, metabolism, excretion, toxicity, and therapeutic potential, *Small*, 2022, **18**, 2106342.
11 C. Li, Y. Wang, H. Nong, X. Hu, Y. Wu, Y. Zhang, C. Liang, K. Chen and S. Li, Manganese and dysprosium codoped carbon quantum dots as a potential fluorescent/T1/T2/CT quadri-modal imaging nanoprobe, *Nanotechnology*, 2022, **33**, 025101.
12 A. Molkenova, M. Kairova, A. Zhussupbekova, K. Zhussupbekov, B. Duisenbayeva, I. V. Shvets and T. S. Atabaev, Carbon dots doped with barium as a novel contrast agent for efficient CT X-ray attenuation, *Nano-Struct. Nano-Objects*, 2022, **29**, 100839.
13 Y. Su, S. Liu, Y. Guan, Z. Xie, M. Zheng and X. Jing, Renal clearable hafnium-doped carbon dots for CT/fluorescence imaging of orthotopic liver cancer, *Biomaterials*, 2020, **255**, 120110.
14 Q. Meng, Y. Wang, C. Li and X. Hu, Bismuth- and gadolinium-codoped carbon quantum dots with red/green dual emission for fluorescence/CT/T_1-MRI mode imaging, *New J. Chem.*, 2022, **46**, 16970–16980.
15 A. Molkenova, A. Toleshova, S. J. Song, M. S. Kang, A. Abduraimova, D. W. Han and T. S. Atabaev, Rapid synthesis of nontoxic and photostable carbon nanoparticles for bioimaging applications, *Mater. Lett.*, 2020, **261**, 127012.
16 B. Zhang, B. Wang, E. V. Ushakova, B. He, G. Xing, Z. Tang, A. L. Rogach and S. Qu, Assignment of core and surface states in multicolor-emissive carbon dots, *Small*, 2022, 2204158.
17 H. Chen, Z. Liu, O. Jiang, J. Zhang, J. Huang, X. You, Z. Liang, W. Tao and J. Wu, Nanocomposite of Au and black phosphorus quantum dots as versatile probes for amphibious SERS spectroscopy, 3D photoacoustic imaging and cancer therapy, *Giant*, 2021, **8**, 100073.
18 H. Chen, Z. Liu, B. Wei, J. Huang, X. You, J. Zhang, Z. Yuan, Z. Tang, Z. Guo and J. Wu, Redox responsive nanoparticle encapsulating black phosphorus quantum dots for cancer theranostics, *Bioact. Mater.*, 2021, **6**, 655–665.
19 Y. Zhuang, S. Han, Y. Fang, H. Huang and J. Wu, Multidimensional transitional metal-actuated nanoplatforms for cancer chemodynamic modulation, *Coord. Chem. Rev.*, 2022, **455**, 214360.
20 H. He, X. Zhang, L. Du, M. Ye, Y. Lu, J. Xue, J. Wu and X. Shuai, Molecular imaging nanoprobes for theranostic applications, *Adv. Drug Delivery Rev.*, 2022, **186**, 114320.
21 A. A. Kajani, L. Rafiee, S. H. Javanmard, N. Dana and S. Jandaghian, Carbon dot incorporated mesoporous silica nanoparticles for targeted cancer therapy and fluorescence imaging, *RSC Adv.*, 2023, **13**, 9491–9500.
22 M. Zheng, S. Liu, J. Li, D. Qu, H. Zhao, X. Guan, X. Hu, Z. Xie, X. Jing and Z. Sun, Integrating oxaliplatin with highly luminescent carbon dots: An unprecedented theranostic agent for personalized medicine, *Adv. Mater.*, 2014, **26**, 3554–3560.
23 S. Saini, H. S. Yaddanapudi, K. Tian, Y. Yin, D. Magginetti and A. Tiwari, Terbium ion doping in $Ca_3Co_4O_9$: A step towards high-performance thermoelectric materials, *Sci. Rep.*, 2017, **7**, 44621.
24 X. Tian and Z. Fan, Comparison between terbium-doped carbon dots and terbium-functionalized carbon dots: Characterization, optical properties, and applications in anthrax biomarker detection, *J. Lumin.*, 2022, **244**, 118732.
25 D. Y. Lu, X. L. Gao and Q. L. Liu, Synergistic effect of terbium and calcium ions on the temperature stability and dielectric loss of $BaTiO_3$-based ceramics, *J. Alloys Compd.*, 2019, **808**, 151713.
26 A. Molkenova, T. S. Atabaev, S. W. Hong, C. Mao, D. W. Han and K. S. Kim, Designing inorganic nanoparticles into computed tomography and magnetic resonance (CT/MR) imaging-guidable photomedicines, *Mater. Today Nano*, 2022, **18**, 100187.
27 **https://nhiso.com/wp-content/uploads/2018/05/ISO-10993-5-2009.pdf**.
28 Y. Y. Liu, Z. X. Sun, J. Liu, Q. Zhang, Y. Liu, A. Cao, Y. P Sun and H. Wang, On the cellular uptake and exocytosis of carbon dots - significant cell type dependence and effects of cell division, *ACS Appl. Bio Mater.*, 2022, **5**, 4378–4389.